Quantum interference of magnetic edge channels activated by intersubband optical transitions in magnetically confined quantum wires

2009 J. Phys.: Condens. Matter 21 025303

(http://iopscience.iop.org/0953-8984/21/2/025303)

J. Phys.: Condens. Matter **21** (2009) 025303 (8pp) doi:10.1088/0953-8984/21/2/025303

Quantum interference of magnetic edge channels activated by intersubband optical transitions in magnetically confined quantum wires

A Nogaret[1], J-C Portal[2,3], H E Beere[4], D A Ritchie[4] and C Phillips[5]

[1] Department of Physics, University of Bath, Claverton Down, Bath BA2 7AY, UK
[2] High Magnetic Field Laboratory, 25 Avenue des Martyrs, 38042 Grenoble, France
[3] Institut Universitaire de France and INSA, 31007 Toulouse, France
[4] Cavendish Laboratory, University of Cambridge, Cambridge CB3 0HE, UK
[5] Department of Physics, Imperial College, London SW7 2AZ, UK

E-mail: A.R.Nogaret@bath.ac.uk

Received 1 September 2008, in final form 22 October 2008
Published 9 December 2008
Online at stacks.iop.org/JPhysCM/21/025303

Abstract
We investigate the photoresistance of a magnetically confined quantum wire in which microwave-coupled edge channels interfere at two pinning sites in the fashion of a Mach–Zehnder interferometer. The conductance is strongly enhanced by microwave power at $B = 0$ and develops a complex series of oscillations when the magnetic confinement increases. Both results are quantitatively explained by the activation of forward scattering in a multimode magnetically confined quantum wire. By varying the strength of the magnetic confinement we are able to tune the phase of electrons in the arms of the interferometer. Quantum interferences which develop between pinning sites explain the oscillations of the conductance as a function of the magnetic field. A fit of the data gives the distance between pinning sites as 11 μm. This result suggests that quantum coherence is conserved over a distance three times longer than the electron mean free path.

(Some figures in this article are in colour only in the electronic version)

1. Introduction

Spatially inhomogeneous magnetic fields provide an alternative means of confining two-dimensional electron systems to electrostatic potentials. The channelling of two-dimensional plasmas has thus been obtained. Commensurability resistance oscillations [1–3] and channelling giant magnetoresistance [4] are examples of semiclassical effects resulting from the guided motion of electron trajectories by a gradient of magnetic field. Diffusive and ballistic transport through magnetic field barriers has equally been investigated [5–10]. The inclusion of the spin degree of freedom in magnetic edge states has recently brought to attention the possibility of exciting spin resonance by driving a current through a gradient of magnetic field [11–13] and the feasibility of polarizing spin currents [14, 15]. While the above effects are semiclassical, quantized energy subbands are anticipated in magnetic dots, superlattices, magnetic barriers and magnetic gradients. To date, the magnetic structure of a magnetic superlattice has been revealed experimentally [16, 17]. The resolution of individual magnetic subbands in magnetic dots and magnetic gradient has been complicated by the fact that magnetic edge states do not ballistically connect to the contacts of a Hall bar, unlike the edge states of the quantum Hall effect. For this reason, it is expected that quantized magnetic subbands could be more easily accessible via optical excitation.

Here, we report quantum interferences in a multi-channel magnetic quantum wire (MCQW) coupled by a microwave field at two pinning sites where electrons experience forward scattering [18, 19]. We use a magnetic field to tune the phase difference between charge density waves propagating in each channel. Their interference give a magnetic field dependent

transmission through the second pining site which we detect through oscillations in the magnetoresistance. Experimental data fit quantitatively the response of a 14 mode channel confined by a spatially varying magnetic field [3, 4] and yield the distance between pinning centres (11 μm) as the only adjustment parameter. This novel type of long range quantum interferences, possibly enhanced by Coulomb interactions, elicits applications to terahertz detectors.

The paper is organized as follows. Section 2 describes the electronic structure of magnetically confined quantum wires. Section 3 reports experimental transport measurements in magnetically confined quantum wires under microwave irradiation. Section 4 interprets and fits the data based on the activation of forward scattering in the MCQW. Section 5 discusses the origin of pinning centres and examines alternative interpretations. Section 6 summarizes the results.

2. Magnetic quantum wires

Magnetically confined quantum wires (MCQW) were obtained by fabricating dysprosium micro-strips of length $L = 40$ μm, width $w = 200$ nm and height $h = 150$ nm at the centre of narrow Hall bars 1.6 μm wide and 32 μm long. A two-dimensional electron gas (2DEG) with density $n_s = 4.0 \times 10^{11}$ cm^{-2} and mobility $\mu = 0.31 \times 10^6$ cm^2 V^{-1} s^{-1} was confined by a shallow GaAs/AlGaAs quantum well set $t = 30$ nm below the surface. Hall bars [9, 10] were fabricated with six pairs of voltage probes spaced by 2, 4, 8 and 16 μm. A magnetic field, B, was applied in the plane of the 2DEG, perpendicular to the long axis of the strip, as shown in the inset to figure 1. Increasing B from zero has the effect of tilting the magnetization, initially along the long axis of the strip, towards the short axis hence increasing the perpendicular magnetization $M_\perp$. As a result, the 2DEG was exposed to a fringing magnetic field, $B_\mathrm{m}(x)$, oriented perpendicular to the plane and varying across the width of the channel. Its peak amplitude increases from 0 to ± 0.9 T when $\mu_0 M_\perp$ increases from 0 to saturation at 3.7 T. The external magnetic field, B, was aligned in the plane to a high accuracy ($<0.8°$) so that it has no direct effect on the 2DEG. An optically transparent titanium film (30 nm thick) capped the magnetic wire to screen residual electrostatic potentials and to protect the dysprosium from oxidation. Samples were cooled to 1.3 K in a variable temperature insert. Microwaves were applied using an over-moded circular waveguide terminated by a linear polarizer ($\vec{E} \perp$ wire). Because the sample was mounted parallel to the magnet axis, a 45° mirror was used to redirect power onto its surface. The output power was varied from 0 to 20 mW using a variable attenuator. The photoresistance was measured under quasi dc conditions using a small current excitation (100 nA) which gave a spectral width ($\sim$0.1 mV) comparable to thermal broadening.

Magnetically confined quantum wires trap 1D magnetic edge states in magnetic field gradients. We obtain the fringing magnetic field semi-empirically using the following magnetostatics formula:

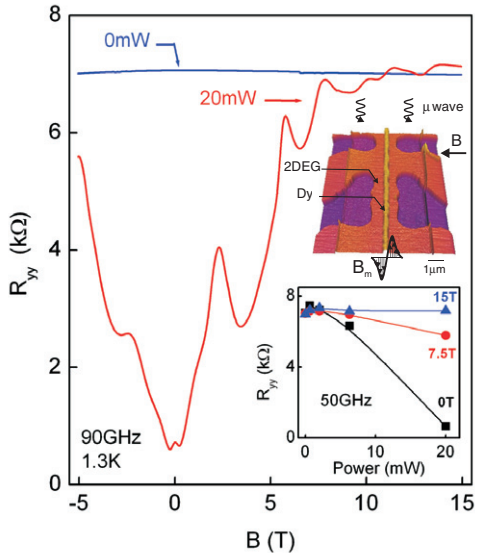

Figure 1. Microwave induced forward scattering. Main panel: resistance of a MCQW (200 nm wide, 24 μm long) with and without microwave irradiation. The resistance at $B = 0$ drops by over an order of magnitude when the microwave power is increased from 0 to 20 mW. Top inset: a MCQW forms in a 2DEG confined laterally by the stray magnetic field, $B_\mathrm{m}(x)$, emanating from a microscopic bar magnet. The external magnetic field, B, is applied in the plane to increase the perpendicular magnetization which in turn increases the depth of the magnetic quantum well. The photoresistance is measured via four-terminal phase-locked detection under microwave irradiation. Bottom inset: dependence of the photoresistance on microwave power at $B = 0$, 7.5 and 15 T. The 0 and 7.5 T traces show a linear resistance decrease. The 15 T curve is essentially flat—only a small increase in resistance due to microwave heating is detectable.

$$B_\mathrm{m}(x) = \frac{\mu_0 M_\perp}{2\pi}\left\{\ln\sqrt{\frac{(x-w/2)^2+(t+h/2)^2}{(x-w/2)^2+(t-h/2)^2}} - \ln\sqrt{\frac{(x+w/2)^2+(t+h/2)^2}{(x+w/2)^2+(t-h/2)^2}}\right\}. \quad (1)$$

Equation (1) is an exact result for an infinitely long stripe of width w, height h which is uniformly magnetized, and stands at distance t from the 2DEG. The depth of the 2DEG is known to within one semiconductor monolayer ($\Delta t/t = 2\%$). The width of fabricated strips fluctuates by 15 nm and the strip height is usually known to better than 5 nm giving experimental errors of $\Delta w/w = 7.5\%$ and $\Delta h/h = 3\%$ respectively. The transverse magnetization is obtained from Hall magnetometry (see below) and is also known to within 5%. For symmetry reasons, the magnetic modulation is independent of the longitudinal magnetization $M_\parallel$. This is why Hall curves only measure $M_\perp$. The precise knowledge of all parameters entering equation (1) suggests that the calculated magnetic field profile will be close to the real one. Hall resistance measurements performed on several dysprosium strips are free from switching behaviour. This suggests the smooth tilting of the magnetization from the longitudinal to the transverse direction. This justifies the use of equation (1)

not only at high B when the magnetization is saturated but also over the whole B range. By insert the experimental magnetization curve, $M_\perp(B)$, in equation (1), we compute the magnetic profile B_m for any value of the applied B.

Since $B_\mathrm{m}(x)$ changes sign at $x = 0$, it follows that the Lorentz force deflects electrons back and forth across the contour of zero magnetic field at the centre of the strip. This binding force derives from a 1D magnetic potential which we now calculate. Using the Landau gauge, the vector potential is given by $A_y(x) = \int_0^x \mathrm{d}\chi\, B_\mathrm{m}(\chi)$ where the origin of the vector potential is set at $x = 0$. The potential energy binding the electron oscillator is given by $V(x, k_y) \equiv \frac{\hbar^2}{2m^*}[k_y + \frac{e}{\hbar}A_y(x)]^2$ where m^* is the electron effective mass and k_y is the electron momentum along the wire. The energy–momentum dispersion curves of a magnetic potential well induced by a step, ramp and spike of magnetic field have been calculated [6, 7]. Here, we refine these calculations by considering the realistic magnetic barrier profile given in equation (1). This has two advantages. Firstly, the observed absorption peaks can be interpreted quantitatively and indexed with specific intersubband transitions. Secondly, equation (1) accounts for the real magnetic edge state structure in the vanishing magnetic modulation of the channel boundaries which was not treated previously. These edge states are peculiar in that they are chiral free electron states. They also differ from the magneto-electric edge states of the quantum Hall effect as they are too weakly confined relative to $k_\mathrm{B}T$ to support ballistic currents. The magnetic potential in figure 2(a) is calculated by assuming that the transverse magnetization is saturated, $\mu_0 M_\perp = 3.67$ T, a situation which is obtained by applying a large B. A quantum well forms at the centre of the channel which is the confining potential of the MCQW. Moving away from the centre of the channel, at $|x| > 200$ nm, the magnetic modulation decreases with the effect that $V(x, k_y)$ tends to the free electron dispersion curve. The central quantum well has depth of 25 meV, sufficient to confine the Fermi sea (14.3 meV), and width of ∼200 nm, which supports energy subbands separated by ∼0.5 meV. The energy subbands $E_n(k_y)$ are plotted in figure 2(b) after numerically solving Schrödinger's equation in potential $V(x, k_y)$.

Transport along the MCQW is ballistic. At the temperature where experiments are conducted, $T = 1.3$ K, the energy spacing between the 12 lowest subbands is $\sim 5k_\mathrm{B}T$ which means that individual subbands can be experimentally resolved. Here k_B is Boltzmann's constant. For negative values of k_y, quantum states split into bonding and antibonding subbands which have different energies but are localized in the same region of space—the MCQW. When k_y increases, bonding and antibonding states become degenerate as they localize in the two potential wells on each side of the MCQW. One therefore has $2N$ magnetic edge states which drift in the negative y-direction at the centre of the MCQW and N counter-propagating free electron states near each edge of the Hall bar. This edge channel picture is summarized in the inset to figure 2(b). A difference with the edge channels of the quantum Hall effect is that, magnetic edge channels are not ballistically connected to voltage probes. Magnetic edge states are sequestered in the MCQW whereas counter-propagating free electron edge states need scattering processes

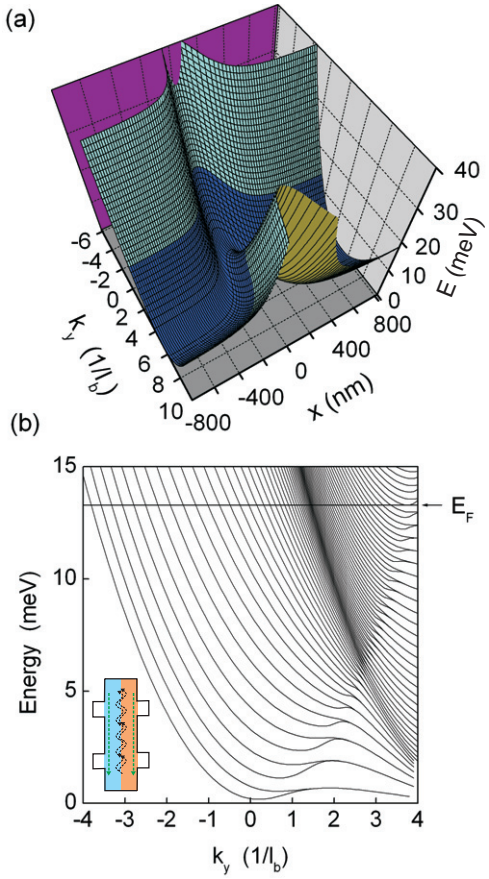

Figure 2. Energy subbands of a magnetically confined quantum wire. (a) Magnetic potential $V(x, k_y)$ induced by the stray magnetic field $B_\mathrm{m}(x)$ when the bar magnet is magnetized to full strength in the perpendicular direction: $\mu_0 M_\perp = \mu_0 M_\mathrm{sat} = 3.67$ T. The MCQW forms in the potential well at the centre of the channel. The Fermi sea is shown in dark blue. (b) Quantum energy subbands $E_n(k_y)$ supported by potential $V(x, k_y)$. Magnetic edge states—bound to the MCQW—are found at the left of the shadowed parabola. To the right, the bonding/antibonding pairs are virtual subbands lying above the MCQW potential barrier. Further to the right, the group velocity changes sign and follows the free electron dispersion curve. Free electron edge states form at the edges of the Hall bar where B_m vanishes. The length scale is $l_b = \sqrt{\hbar/e} = 25.7$ nm. Inset: edge states in magnetically modulated Hall bar.

to remain in thermal equilibrium with the contacts. At low temperature, these states are more likely to conduct through optical activation. Chiral free electron edge state are more weakly confined than MCQW subbands. In fact, the top right quadrant of figure 2(b) shows energy gaps becoming smaller than $k_\mathrm{B}T$ which suggests that free electron edge states will be smeared into a continuum. It is therefore anticipated that, at 1.3 K, transport will be ballistic inside the MCQW and diffusive elsewhere.

MCQWs present a number of advantages over electrostatic quantum wires: the depth of the magnetic well is continuously tunable from zero to about 25 meV. Equation (1) states that the magnetic modulation is proportional to $M_\perp$ hence it is sufficient to know the magnetization curve to obtain the dependence of the magnetic potential on B. The magnetic potential modifies the Fermi surface without affecting the electron density and mobility unlike for electrostatic potentials.

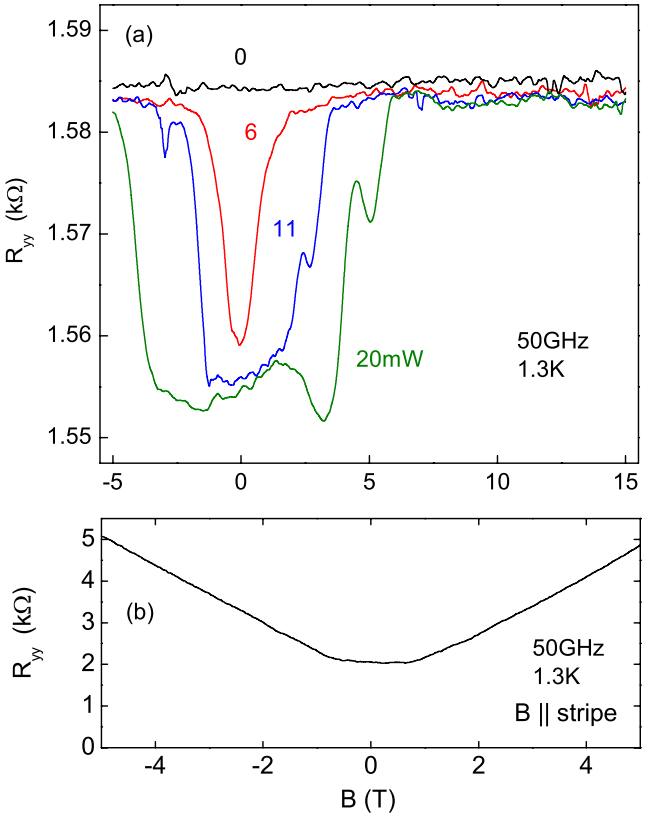

Figure 3. (a) Photoresistance of the MCQW measured across voltage probes separated by 4 μm. When microwave power increases from 0 to 20 mW, the $B = 0$ resistance drops by 2%. (b) The same measurement when B is rotated by 90° in order to magnetize the stripe along its long axis. The contact spacing is now 12 μm.

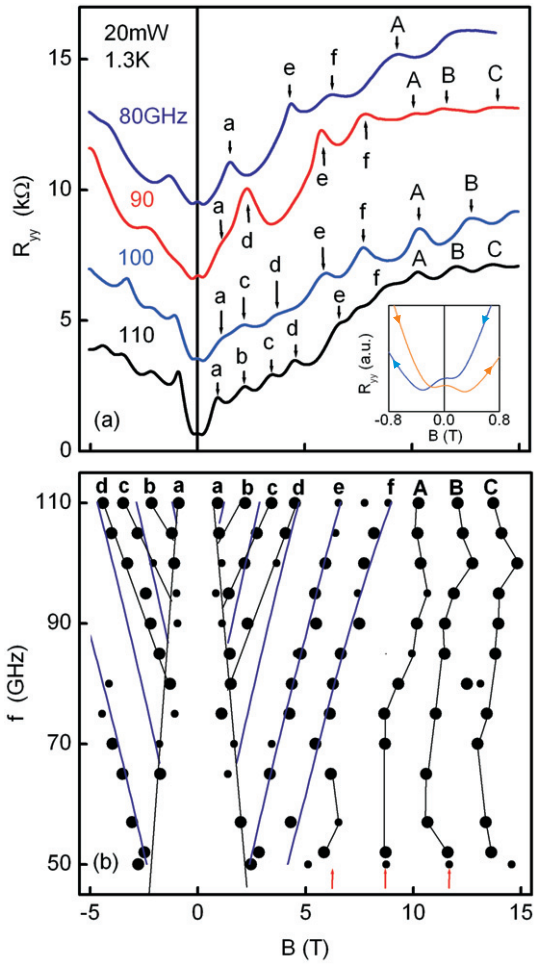

Figure 4. Frequency dependence. (a) The longitudinal resistance displays two series of oscillations. The low field series (a, b, c, d, . . .) has peaks which move linearly with f. The peaks in the high field series (A, B, C . . .) fluctuate about an average value which is independent of frequency. Curves are vertically offset by 3 kΩ. Inset: magnetization reversal of dysprosium as evidenced by the longitudinal magnetoresistance. (b) Fan chart of peak positions. The dot size indicates the amplitude of experimental peaks. The blue lines are the theoretical fan fitted to the low field series. The red arrows indicate the theoretical peak positions of the high field series—see the text.

3. Experimental results

Figure 1 shows the resistance of the MCQW with and without microwave irradiation when measured across voltage probes separated by 24 μm. The zero-field resistance drops by over an order of magnitude from 7.1 to 0.6 kΩ when microwave power increases from 0 to 20 mW ($\Delta R/R = -92\%$). In comparison, the unmodulated Hall bar in the dark has resistance of 0.18 kΩ; a value consistent with the resistance of a channel of nominal width supporting 75 modes. It therefore appears that the resistance of the magnetically modulated channel drops by over an order of magnitude when microwaves are switched on. In contrast the resistance drops across voltage probes separated by 4 μm is much smaller. Figure 3(a) shows that $\Delta R/R = -2\%$ at maximum microwave power. The magnitude of the photoresistance therefore appears to increase with the wire length. The magnetoresistance shows a rich and complex structure with B applied *in the plane*. We demonstrate that these oscillations arise from the magnetic potential by rotating the applied B by 90° to align it parallel to the stripe. The magnetoresistance without magnetic modulation varies monotonically as shown in figure 3(b). The stripe being magnetized along its long axis, the magnetic modulation vanishes and correspondingly, oscillations disappear. This behaviour is consistent with the magnetoresistance of the unmodulated 2DEG in an in-plane magnetic field under microwaves [18]. The most notable features are two series of magnetoresistance oscillations and the return of the resistance to its level prior to irradiation when $B > 9$ T. The photoresistance at constant B is shown in the inset to figure 1. The photoresistance drops linearly with microwave power for $B = 0$ and 7.5 T. By contrast, the $B = 15$ T curve is independent of microwave power.

Figure 4(a) displays magnetoresistance oscillations at microwave frequencies between $f = 80$ and 110 GHz. The observed oscillations arise from the spatially varying magnetic field, $B_m(x)$ whose strength increases with B. This assertion is based on the observation that the magnetoresistance curve changes amplitude depending on the direction of field sweep. The hysteresis effect is associated with magnetization reversal in the finger gate, see inset to figure 4(a). Secondly, figure 3(b) shows that the device exhibits no magnetoresistance when

the magnetization is longitudinal (no modulation). The fan diagram in figure 4(b) maps the position of individual peaks in the f–B plane. One distinguishes two series of oscillations. The low magnetic field series has peaks labelled (a–f) whose positions vary linearly with f. Peak (a) moves to lower magnetic field whereas peaks (b–f) move to higher magnetic field. Peaks (A, B, C) are distinguished from the first series by being independent of microwave frequency. Fluctuations in the peak positions of the (A, B, C) series arise because the transverse magnetization is nearly saturated-to within 4%. Near saturation, the slope of the magnetization curve is nearly flat. Small fluctuations in magnetization between sweep up and sweep down traces will be corrected by applying a magnetic field much larger than for identical fluctuations taking place at low magnetic field where the magnetization curve is steeper. This explains the wobbling of peaks at high B in figure 4(b).

4. Interpretation

The photoresistance and magnetoresistance data can be interpreted in a coherent way by assuming a 1D correlated electron system pinned by scatterers. These weak links are most likely to arise from unintentional defects in the finger gate which locally relax magnetic confinement. At these points, the smaller energy separation between magnetic subbands allows microwave absorption over a wide range of microwave frequencies. Topological defects, either magnetic or originating from impurities, are smooth on the scale of the Fermi wavelength (≈1 nm) hence satisfy the adiabatic condition that allows forward scattering under microwave irradiation [20]. In the absence of microwaves, pinning centres backscatter electrons. This is because they accumulate electric charge which blockades quantum tunnelling at weak links, an effect which is enhanced by Coulomb interactions [21, 22].

A sophisticated theory of microwave absorption in multimode channels has been constructed by Krive *et al* [20]. These authors show that dipole-like charge density perturbations created by *intersubband* transitions renormalize the tunnelling rates through pinning centres. Under conditions where subbands involved in the transition have different velocities, these electric dipoles enable the tunnelling of charge density waves across pinning centres. If the microwave heating is inhibited as a result of a perturbation applied to the system, forward scattering will be switched off and the resistance will return to its level in the absence of irradiation. This is precisely what happens at high magnetic field. Increasing B increases the energy gaps between magnetic subbands in the MCQW to the point where they become too large to absorb a microwave photon. The quantitative analysis done below sets the absorption edge at 8 T at 90 GHz which matches the onset of the resistance plateau seen in figure 1.

Forward scattering reveals itself in more dramatic fashion in the magnetic field dependence of the resistance which we now describe. MCQWs have chiral edge states which by definition circulate in only one direction. This has the consequence that charge density excitations circulating along parallel channels will interfere in the fashion of a Mach–Zehnder interferometer if each path splits at one pinning centre and interact again at the next. This interferometer is shown in figure 5(a). Two weak links pin the electron channel at y and $y + d$. In the absence of microwaves, these pinning sites block transmission and cause charge accumulation as reported above. However in the presence of a microwave field tuned at the frequency of the inter-mode electron transition, electric dipoles allow a finite tunnelling probability through the pinning sites [12, 13]. Two hybridized charge density waves propagate between y and $y + d$. These have velocity given by:

$$s_{\pm} = \frac{v_{\mathrm{lF}} + v_{\mathrm{uF}}}{2} + \frac{V_0}{\pi\hbar} \pm \frac{v_{\mathrm{lF}} - v_{\mathrm{uF}}}{2}\sqrt{1 + K^2} \qquad (2)$$

where v_{lF} and v_{uF} are the Fermi velocities of the lower and the upper channel, $V_0 \cong e^2/4\pi\varepsilon$ is the Coulomb interaction and $K = V_0/\hbar(v_{\mathrm{lF}} - v_{\mathrm{uF}})$ is the effective coupling strength between channels [19]. ε is the dielectric constant of GaAs and e is the electron charge. When B_{m} is maximum, one obtains $K = 18$. Since K will invariably increase for smaller B_{m}, the MCQW belongs to the strong coupling regime: $K \gg 1$. In which case, the speed of hybridized charge density waves is independent of $(v_{\mathrm{lF}} - v_{\mathrm{uF}})$ hence independent of the magnetic field. These modes decay as $d^{-\lambda}$ where $\lambda_{\pm} \equiv 1 \pm K/\sqrt{1 + K^2}$. The mode, λ_{-}, clearly dominates and is retained for fitting the peak positions. Theory predicts that this mode will absorb microwave power according to a $\sin(\Phi)$ function [19] where $\sin(\Phi)$ is the phase factor given in the left-hand side of equation (3). Maxima of power absorption occur when:

$$(k_{\mathrm{lF}} - k_{\mathrm{uF}} - 2\pi f/s_{+})\, d + \frac{\pi}{2}\frac{K}{\sqrt{1 + K^2}} = \frac{\pi}{2} + 2n\pi \qquad (3)$$

where n is an integer and $k_{\mathrm{lF}} - k_{\mathrm{uF}}$ is the difference of Fermi wavevector of the lower and upper channels. The $k_{\mathrm{lF}} - k_{\mathrm{uF}}$ term carries the dependence on B. Hence equation (3) describes a fan diagram in the f–B plane that has parallel branches, each indexed by n.

A quantitative fit of the experimental data requires knowing the magnetization curve $M_{\perp}(B)$. Figure 5(b) shows the magnetization curve measured by Hall magnetometry. The experimental curve is interpolated with the function shown in the caption. The latter is used to calculate the B-dependence of energy levels, shown in figure 5(c), and the B-dependence of $k_{\mathrm{lF}} - k_{\mathrm{uF}}$. Inserting the latter into equation (3) gives the *slope* of every branch in the fan without any adjustment parameter. In contrast, the spacing of two consecutive branches, n and $n + 1$, depends on distance d which we can extract from a fit to the data. The best fit to figure 4(b) gives $d = 11 \pm 0.5\ \mu$m (blue lines). This implies that quantum interferences take place over a distance three times larger than the electron mean free path. The magnetic edge channel picture also explains why the fan only appears at low B. The energy gaps between MCQW subbands increase with B up to the point where interchannel transitions are forbidden by energy conservation. The theoretical absorption edge obtained from figure 5(c) runs from 4.5 T at 50 GHz to 8.0 T at 110 GHz. This fits very nicely the upper boundary of the experimental fan in figure 4(b).

We finally address the origin of the high magnetic field series. This series is non-resonant (as independent of f) and

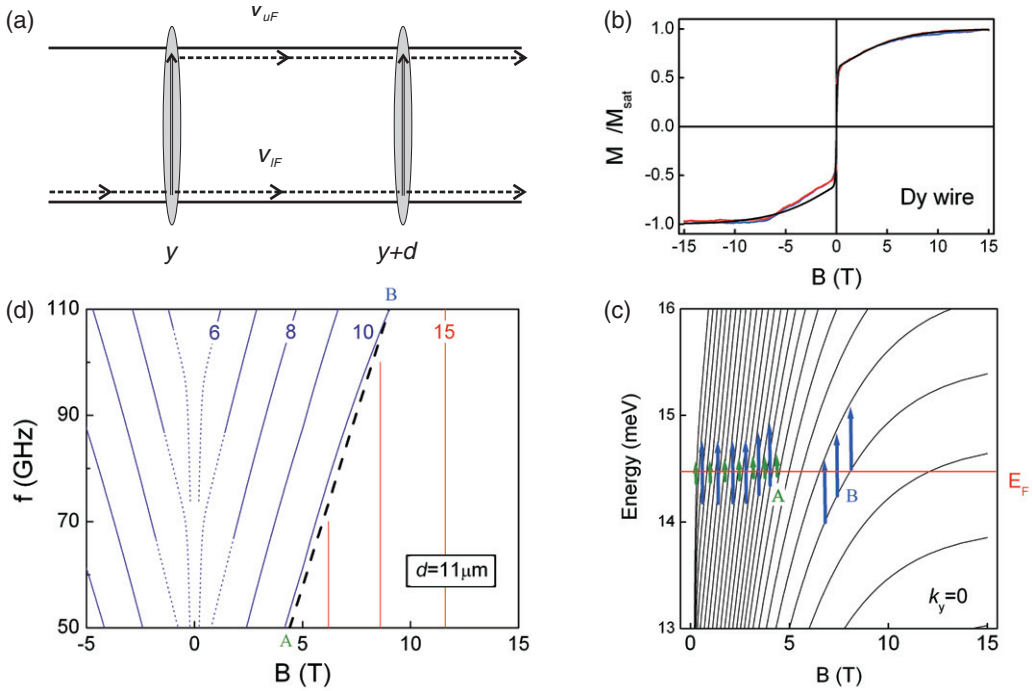

Figure 5. Quantum interferences of magnetic edge channels in MCQW. (a) Resonant microwave absorption couples two channels and enhances forward scattering at weak links (e.g. impurities) located at y and $y + d$. Electron transmission through the interferometer depends on the difference in Fermi wavevectors and Fermi velocities of the lower and upper channels. (b) Transverse magnetization curve of a dysprosium bar—the up/down sweeps correspond to the blue/red curves. Theoretical fit: $M_\perp/M_{\rm sat} = 0.6\tanh(8B) + 0.4\tanh(0.16B)$ (black curve). (c) Quantum energy levels $E_n(k_y = 0, B)$ calculated as a function of the *applied magnetic field* using the empirical magnetization curve. Blue (green) arrows show the electron transitions allowed at 110 GHz (50 GHz). B (A) is the upper limit of microwave absorption at 110 GHz (50 GHz). (d) The theoretical fan chart shows the microwave absorption frequencies of the two-mode as a function of the magnetic field. The absorption maxima are labelled $n = 6, 7, 8, 9, 10$ (blue curves) and $n = 13, 14, 15$ (red curves) as explained in the text. The dotted line (A–B) is the absorption edge. The distance $d = 11$ μm is the only adjustment parameter in the theory.

may be ascribed to charge density waves excited indirectly, perhaps in the contacts. Setting $f = 0$ in equation (2) allows to calculate the maxima of microwave absorption as a function of n. The resulting theoretical positions are the red arrows in figure 4(b) which fit the experimental lines. We summarize our findings by mapping the theoretical peak positions in figure 5(d). These replicate the major features of the experiment.

5. Discussion

The above interpretation rests on the existence of weak links whose origin should be clarified. High resolution electron micrographs and topographic profiles of the magnetic strip were taken. The latter, in figure 6, shows that the width of the finger gate fluctuates by 15 nm at the top whilst sidewalls become smoother closer to the base. These fluctuations are too weak to give micro-widenings absorbing microwaves continuously over the 75–110 GHz frequency range. Besides the correlation length of edge roughness, ∼300 nm, is too small to explain the 11 μm spacing between pinning centres. A more plausible explanation is the local weakening of the magnetic structure. This can occur for reasons such as the build-up of strain at the semiconductor/dysprosium interface or the contamination of dysprosium by exposure to air.

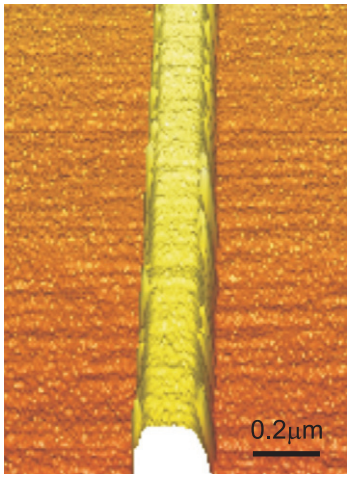

Figure 6. High resolution AFM scan of the magnetic strip showing edge roughness.

If one ignores the existence of pinning centres, what are the other possible sources of resistance oscillations? Fitting the data with a single particle picture suffers the following objections. Firstly, a local relaxation of the magnetic potential perturbs the transmission of all edge channels in the same way. The transfer of an electron from one subband to another

which has the same conductance will not change the overall conductance. Unless the transition occurs between a localized and an extended state, the overall conductance does not change. Secondly, the amplitude of oscillations is too large to be explained in terms of resonant microwave absorption. One also sees in figure 2(b) that $E_n(k_y)$ curves are gapless and several pairs of subbands are simultaneously tuned to the same photon energy. Microwaves are thus absorbed continuously over a range of photon energies and magnetic fields up to the absorption edge. The amplitude of the observed oscillations is consistent with charge density waves.

We have also considered *classical edge plasmons* as a second possible explanation. The voltage contacts of the Hall bar break the translational invariance of the 2DEG and create oscillating electric dipoles which emit plasma waves. A perpendicular magnetic field causes the circulation of these plasma waves near the edge of the Hall bar in a direction determined by the sign of the magnetic field. Kukushkin *et al* [23] have shown that edge plasmons emitted by two contacts will interfere constructively or destructively depending on whether an even or odd number of half-wavelengths fit between them. The perpendicular magnetic field reduces the plasmon velocity as $\propto 1/B$ hence changes the interference conditions as more half-wavelengths fit in the distance between contacts. In our sample, the distance between contacts is however much smaller than the plasmon wavelength. In [19], contacts separated by $L = 0.5$ mm support oscillations with a period of 200 mT at $f = 53$ GHz. Since the period scales as $\propto n_s/fL$, edge magneto-plasmon oscillations in our system would have period of 2.9 T across 24 μm contacts at $f = 100$ GHz. Not only is this period far larger than the period of our measured oscillations but the field orientations are different. The perpendicular magnetic field at the edges of our sample is zero (it remains less than ± 100 mT until half-distance from the centre). Hence the formation of edge magneto-plasmons can be entirely ruled out.

6. Conclusion

In summary, we have measured microwave activated transport in a two-dimensional electron system confined by a spatially varying magnetic field. The magnetic potential quantizes electrons in ballistic edge channels as demonstrated by the existence of an absorption edge in the magnetoresistance. Namely, microwave absorption is suppressed when the intersubband energy becomes larger than the photon energy. The observed photoresistance and magnetoresistance oscillations both arise from the activation of forward scattering at pinning sites in the wire. These pinning sites cause individual modes to interfere with the effect of modulating the wire conductance. By varying the strength of the magnetic potential, we have tuned the Fermi wavevector of individual quantum subbands and controlled the phase of plasma waves in the interferometer. This physical picture quantitatively fits the data with a single adjustment parameter which is the distance between pinning sites.

Acknowledgments

We thank V I Fal'ko, I Krive, R Shekhter and L Gorelik for discussions. The support of the EPSRC(UK) EP/E002390 and the Transnational Access—Specific Support Action Programme—Contract RITA-CT-2003-505474 of the European Commission is gratefully acknowledged.

References

[1] Izawa S, Katsumoto S, Endo A and Iye Y 1995 Magnetoresistance oscillation in 2-dimensional electron gas under spatially modulated vector potential *J. Phys. Soc. Japan* **64** 706
[2] Ye P D, Weiss D, Gerhardts R R, Seeger M, von Klitzing K, Eberl K and Nickel H 1995 Electrons in a periodic magnetic field induced by a regular array of micromagnets *Phys. Rev. Lett.* **74** 3013
[3] Carmona H, Geim A K, Nogaret A, Main P C, Foster T J, Henini M, Beaumont S P and Blamire M G 1995 2-dimensional electrons in a lateral magnetic superlattice *Phys. Rev. Lett.* **74** 3009
[4] Nogaret A, Bending S J and Henini M 2000 Resistance resonance effects through magnetic edge states *Phys. Rev. Lett.* **84** 2231
[5] Muller J E 1992 Effect of a non-uniform magnetic field on a 2-dimensional electron gas in the ballistic regime *Phys. Rev. Lett.* **68** 385
[6] Reijniers J and Peeters F M 2000 Snake orbits and related magnetic edge states *J. Phys.: Condens. Matter* **12** 9771
[7] Sim H S, Chang K J, Kim N and Ihm G 2001 Electron and composite fermions edge states in non-uniform magnetic fields *Phys. Rev.* B **63** 125329
[8] Vancura T, Ihn T, Broderick S, Ensslin K, Wegscheider W and Bichler M 2000 Electron transport in a two-dimensional electron gas with magnetic barriers *Phys. Rev.* B **62** 5074
[9] Bae J U, Lin T Y, Yoon Y, Kim S J, Imre A, Porod W, Reno J L and Bird J P 2008 Large tunnelling magnetoresistance in a field-effect transistor with nanoscale ferromagnetic gate *Appl. Phys. Lett.* **92** 253101
[10] Cerchez M, Hugger S, Heinzel T and Schulz N 2007 Effect of edge transmission and elastic scattering on the resistance of magnetic barriers *Phys. Rev.* B **75** 035341
[11] Nogaret A 2007 Electrically induced Raman emission from planar spin oscillator *Phys. Rev. Lett.* **94** 147207
[12] Nogaret A and Peeters F M 2007 Electrically induced spin resonance fluorescence. I Theory *Phys. Rev.* B **76** 075311
[13] Nogaret A, Lambert N J and Peeters F M 2007 Electrically induced spin resonance fluorescence. II Theory *Phys. Rev.* B **76** 075312
[14] Wrobel J, Dietl T, Lusakowski A, Grabecki G, Fronc K, Hey R, Ploog K H and Shtrikman H 2004 Spin filtering in hybrid ferromagnetic-semiconductor structure *Phys. Rev. Lett.* **93** 246601
[15] Frustaglia D, Hentschel M and Richter K 2004 Aharonov–Bohm physics with spin. II. Spin-flip effects in two-dimensional ballistic systems *Phys. Rev.* B **69** 155327
[16] Edmonds K W, Gallagher B L, Main P C, Overend N, Wirtz R, Nogaret A, Henini M, Marrows C H, Hickey B J and Thoms B 2001 Magnetoresistance oscillations due to internal Landau band structure of a two-dimensional electron system in a periodic magentic field *Phys. Rev.* B **64** 041303
[17] Shi J R, Peeters F M, Edmonds K W and Gallagher B L 2002 Even–odd transition in the Shubnikov de-Haas oscillations in a two-dimensional electron gas subjected to periodic magnetic and electric modulations *Phys. Rev.* B **66** 035328

[18] Yang C L, Du R R, Pfeiffer L N and West K W 2006 Influence of a parallel magnetic field on the microwave photoconductivity in a high mobility two-dimensional electron system *Phys. Rev.* B **74** 045315
[19] Gorelik L Y, Krive I V, Kulinich S I, Shekter R I and Jonson M 2002 Interaction-enhanced interference effects in a Luttinger liquid *Europhys. Lett.* **57** 409
[20] Krive I V, Kulinich S I, Gorelik L Y, Shekter R I and Jonson M 2001 Interchannel transitions in a Luttinger liquid *Phys. Rev.* B **64** 045114
[21] Matveev K A and Glazman L I 1993 Coulomb blockade tunnelling into a quasi-one-dimensional wire *Phys. Rev. Lett.* **70** 990
[22] Kane C L and Fisher M P A 1992 Transport in a one channel Luttinger liquid *Phys. Rev. Lett.* **68** 1220
[23] Kukushkin I V, Akimov M Yu, Smet J H, Mikhailov S A, von Klitzing K, Aleiner I L and Fal'ko V I 2004 New type of B-periodic oscillations in a two-dimensional electron system induced by microwave radiation *Phys. Rev. Lett.* **92** 236803